Available online at www.sciencedirect.com
SCIENCE DIRECT
Cement and Concrete Research 36 (2006) 504 – 520
Cement and Concrete Research

Corrosion damage diagnosis of a reinforced concrete beam after 40 years natural exposure in marine environment

O. Poupard [a], V. L'Hostis [b,*], S. Catinaud [c], I. Petre-Lazar [d]

[a] Laboratoire Pierre Sue, CNRS/CEA Saclay, bât. 637, 91191 Gif-sur-Yvette, France
[b] Laboratoire d'Etude du Comportement des Bétons et des Argiles, CEA Saclay, DEN/DPC/SCCME/LECBA, bât. 158, 91191 Gif-sur-Yvette Cedex, France
[c] Centre d'Expertise du Bâtiment et des Travaux Publics, Domaine de Saint Paul, 78470 Saint Rémy les Chevreuse, France
[d] EDF/DRD/MMC, Les Renardières, Route de Sens—Ecuelles, 77250 Moret sur Loing Cedex, France

Received 23 March 2005; accepted 7 November 2005

Abstract

A detailed investigation of the chloride induced corrosion damage was performed on a 40 years old reinforced concrete beam exposed in marine environment. Visual observations, electrochemical measurements, carbonation depth, total chloride content were carried out. Half-cell potential measurements were used to locate corrosion areas. It appeared that the interpretation based on gradient of the potential was in good concordance with real state of damage. Complementary destructive methods are applied to observe the real corrosion state of steel rebars and characterize the corrosion products and the steel/concrete interface (optical and electronical microscopy tools (XRD, SEM, EDS and μ-Raman).

All these data indicate that on the beam, one may distinguish two types of areas: "high-corrosion zones" and "low-corrosion zones." Given the fact that the "high corrosion zones" were found to be close to corrosion induced cracks and that they have a different morphology, this contribution concludes that the position of these areas did not shift in time.

Keywords: Characterization; Corrosion; Long-term performance; Chloride; Reinforcement

1. Introduction

Corrosion of reinforcing steel bars is of great concern because it is the most widespread cause of degradation in reinforced concrete structures. Initially, steel embedded in concrete is naturally protected from corrosion by the alkalinity of its pore solution (12.5 and higher) [1–3]. This high alkalinity enables the formation of a passive film on the rebar surface which prevents the development of an active corrosion process. However, this passive state can be inhibited by the destruction of the protective film by aggressive ions (chlorides) or by an acidification of the environment in the vicinity of the rebar (carbonation). In marine environment, reinforcing steel corrosion is the natural result of the chloride penetration in concrete cover. Under these conditions, depassivation of steel rebars can lead to the localized formation of porous oxide layers at the steel/concrete interface. As iron oxides layers have a volume twice to four times higher than iron volume, stresses can be generated within the concrete and create irreversible damage of the structure [4–6]: (i) cracking of concrete (ii) carrying capacity loss (iii) and finally ruins of the structure.

The detrimental effect of corrosion on the service life of reinforced concrete structures has implied the development of various research projects in different domains [7–16]: description of electrochemical processes in reinforcing steel/concrete system, favourable corrosion conditions, transport mechanisms and kinetics of aggressive species, mechanical consequences and monitoring tools.

Most of the studies on corrosion of reinforced concrete structures are issued from laboratory tests. Few data are also available under accelerated exposure conditions in controlled environment. However these tests are not devoted to be representative to the "in situ" behaviour. Investigations on the damage state of reinforced concrete structure exposed to long-term exposure under "in situ" environment are scarce in

* Corresponding author. Tel.: +33 169 08 32 13; fax: +33 169 08 84 41.
E-mail address: lhostis@azurite.cea.fr (V. L'Hostis).

0008-8846/$ - see front matter © 2005 Elsevier Ltd. All rights reserved.
doi:10.1016/j.cemconres.2005.11.004

literature. Now these long-term studies are essential to improve the understanding of the corrosion mechanisms as well as the rates of deterioration.

A first important point considering long-term exposure in aggressive environment is to assess an accurate overview of corrosion state within reinforced concrete structures. During the past decades, some non destructive methods have been developed. Of these methods, electrochemical measurements (potential mapping, corrosion rate measurement) seem very promising. The actual methods are always in development phase and no general agreement has been reached about the accuracy of these methods and their reliability on in situ conditions.

Another important issue still under discussion concerns the characterization of corrosion products in reinforced concrete. Some field experiences were performed on long-term exposure in atmospheric environment [17,18]. Duffo et al. [17] characterized the corrosion products at the steel/concrete interface for 65 years old specimens exposed to atmospheric environment. They observed magnetite close to the rebar and a mix of goethite and calcite in the external area. However, the authors only use characterization methods at macro-level (XRD and transmission Mössbauer spectroscopy). Chitty et al. [18] studied archaeological analogues corrosion systems taken from different buildings aged from 80 to 1700 years old. A complete characterization based on macro and microscopic methods has been performed. They highlighted that the steel/binder interface presented a similar pattern for all sites studied: metallic substrate, dense product layer, transformed medium and binder. The dense product layer is mainly made of goethite with magnetite and/or maghemite marblings. In all the case studies, samples are exposed to atmospheric environment, corrosion process being mainly due to carbonation attack. At our knowledge no such data are available for corrosion due to chloride attack.

2. Objective

Based on these considerations, this paper presents an experimental program that characterises the corrosion damage on a prestressed concrete beam (structure size element) exposed during 40 years in a natural marine environment by studying:

- The initiation factors of the corrosion process,
- The geometrical distribution of the damaged zones and factors influencing this distribution,
- The precision of detecting the damaged zones by Non Destructive Techniques,
- The local characterisation of the corrosion products and steel–concrete interface patterns by coupling of optical and electronical microscopy tools (XRD, SEM, EDS and μ-Raman).

The originality of this contribution is to perform a detailed diagnostic on a long time natural exposed specimens. The reported data are relevant as an experimental reference for quantitative models used in long time service life predictions and maintenance optimisation for structures in marine environment.

3. Materials and methods

3.1. Exposure conditions

The studied prestressed concrete beam was cast and stored during about 40 years in a tidal marine zone (firstly on a site near Rance's dam (Britain, France) until 1976, then on IFREMER site at Sainte Anne de Portzic (Britain, France) in similar conditions until 2000).

3.2. Description of the beam

Dimensions of the beam are $2500 \times 200 \times 200$ mm. The ends (on 250 mm) are protected by a bituminous binder. Fig. 1 presents the layout details of the beam. It is reinforced with 10 passive plain steel bars (∅ 6 mm) and 10 stirrups (∅ 6 mm) spaced at 250 mm. The concrete cover thickness of the passive reinforcing steels is 16 mm on the 4 sides. The four sides of the beams are noted (T) for the top side (B) for bottom side and (L) and (R) for left and right sides. Fig. 2 illustrates the anchorage device of prestressed wires.

The beam is prestressed from two prestressing wires. These wires are composed of high-strength steel bars (∅ 7 mm) embedded in plastic gains (∅ 12 mm) injected with "grease." They are moved off centre in the lower part of the beam as indicated on Fig. 1. So it can so be considered that the prestress application allows to reproduce cracking pattern similar to a load applied to a structure during long-term exposure. Initially, when the tensions were applied to the beam, the longitudinal stresses in the concrete were 2.3 MPa (in tension) and 7.1 MPa (in compression) in the upper and lower part of the beam, respectively.

The cement used is CPAL 210–325. It would correspond to a classical cement CEM II/A (CPJ) with 65% of clinker and 35% of secondary constituents (with a percentage in slags about 10–20% in cement mass). The gravels (15/25 mm and 5/15 mm) and sand (0/5 mm from Seine River, France) are used as coarse and fine aggregates. Table 1 summarizes the mix proportions of concrete. The average compressive strength obtained on cylinder specimens at 28 days was 30 MPa.

3.3. Methodology

First, a visual observation is carried out to obtain a general overview of the damage state of the beam. Then, electrochemical measurements are performed to evaluate in a non-destructive way the corrosion state of reinforcing steels within the structure (corrosion potential and corrosion rate). Finally, destructive measurements are performed to visualize the real damage state of reinforcing steel and to characterize corrosion products properties. The carbonation depth and

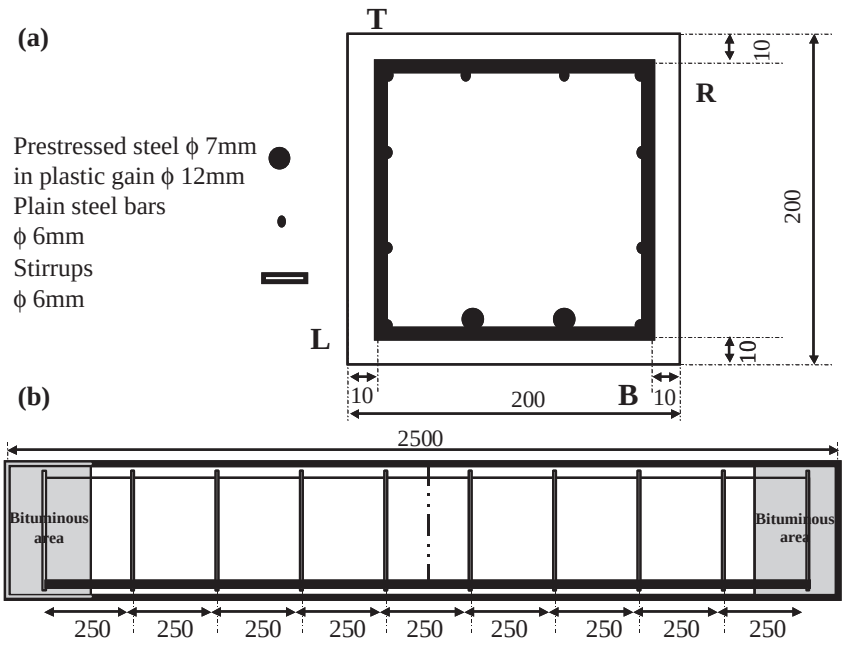

Fig. 1. Layout details of the beam.

chloride content are also estimated in order to know the corrosion origin.

3.4. Methods

3.4.1. Visual observation-crack maps

For each side, crack maps are drawn, focusing on locations of longitudinal cracks due to the corrosion attack. On these maps lengths and widths of each referred crack are also indicated.

3.4.2. Carbonation and chloride content analyses

The carbonation depths are measured on the beam by a phenolphthalein test. For this purpose, freshly splits concrete surface are sprayed with a phenolphthalein solution at various locations along the beam. Sound concrete is coloured red by the indicator while the colour of carbonated concrete remains unchanged. This change occurs in the pH range 8.3–10.

The total chloride concentration measurements have been performed in 1998 from AFPC-AFREM recommendations [19]. Two samples (noted C_1 and C_2) are taken from 2 locations along the tensile area (side T). The extractions of "total" chlorides are obtained by mixing 5 g concrete powder with saturated nitric acid. The analyses are performed by a potentiometric titration. Total chloride content is expressed in percent mass cement. The cement content is estimated by considering the soluble siliceous concentration in the powder samples (measured from atomic absorption). It was supposed that soluble silicieous content of the used cement was about 20%.

Fig. 2. Photography of anchorage device for prestressing steel wires.

3.4.3. Electrochemical analysis

Electrochemical measurements are performed on the beam to evaluate in a non-destructive way the rebar corrosion activity within the structure. First, half-cell potentials are measured. The principle of this method is based on the measurement of the potential difference between rebars and a reference electrode. A multi-electrode device Canin® is used to collect data (three measurement lines per side and one reading per centimeter along the beam length). The reference electrode is a copper/saturated copper sulphate (CSE: +318 mV/NHE). Measurements are performed according to Rilem recommendations [14].

The measurement of half-cell potential is a qualitative way to assess the corrosion state of reinforcing steel and to locate the steel area which presents high corrosion probability. To characterize in a quantitative way the corrosion activity on reinforcing steel surface, it is essential to evaluate the corrosion rate. The corrosion rate, v_{corr}, is deduced from the

Table 1
Concrete mix composition and properties

Cement (kg m^{-3})	Water (kg m^{-3})	e/c	Granulometry (kg m^{-3})			Slump test (cm)	Total free water porosity at 28 days (in percent of the total volume)
			Sand 0/5 mm	Gravel 10/25 mm	Gravel 5/15 mm		
400	210	0.53	550	930	290	5–7	17

polarization resistance (R_P) measurement [15]. The current density, I_{corr}, is then obtained from Stern and Geary equation (Eq. (1)) [20]:

$$I_{corr} = \frac{B}{R_P} \quad (1)$$

with B a constant parameter which varies from 13 to 52 mV depending on the studied system. In this study, B will be equal to 26 mV (if R_P and I_{corr} are expressed respectively in kiloohms and microamperes), according to Rilem recommendations [20].

The corrosion rate can be deduced from corrosion current from Faraday equation (Eq. (2)):

$$I_{corr} = \frac{z\rho F}{w_a I}\frac{dV}{dt} \quad (2)$$

where $\frac{dV}{dt}$ is the evolution of dissolved volume during time, w_a is the Fe atomic molar mass (w_a=56 g mol^{-1}), I_{corr} is the corrosion current (A), z is the number of electrons transferred per iron atom (z=2 for $Fe \rightarrow Fe^{2+}+2e^-$), ρ is the steel density (ρ=7.85 g cm^{-3}) and F is the Faraday constant parameter (F=96,500 C).

If corrosion current is expressed in microamperes, corrosion rate in micrometers per year is given by the following relation (Eq. (3)) assuming uniform corrosion across the bar surfaces:

$$V_{corr} = 11.6\frac{I_{corr}}{A} \quad (3)$$

where A is the steel surface area (in square centimeters).

Electrochemical measurements are performed with a Gamry Potentiostat. A specific sensor electrode is used to apply the corrosion potential and the over-potential during the measurements. It includes a reference electrode (CSE) and a stainless steel mesh as counter-electrode (50 × 90 mm). The electric contact is ensured by a wetted sponge. No polarization confinement is applied. Area A in Eq. (3) corresponds to the reinforcing steel area under the electrode sensor (about 15 cm^2). The following procedure is adopted for R_P measurement:

- the stability of the half-cell potential is first controlled (stability is considered when deviation is lower than 1 mV during a 60 s period),
- the polarisation resistance is measured by a potentiodynamic scanning (from $E_{corr}-10$ mV to $E_{corr}+10$ mV with a scan rate of 0.166 mV/s) [20],
- the electrical resistance (R_e) is evaluated from impedance measurement (by applying a small sinusoidal perturbation (amplitude 10 mV)) in the high-frequency domain (from 100 kHz to 10 Hz)). This measure allows to take into account the IR drop in the corrosion rate estimation.

Corrosion rates are measured on the upper and lower sides (T and B, respectively). Measurements are selected from potential map according to Rilem recommendations TC-154-EMC [15]. On the top side, four points are chosen: three on an active area and one point on a passive area. On the bottom side, two points are chosen: one on an active area and the other on a passive area.

3.4.4. Characterization of corrosion pattern

The methodology proposed during archaeological analogues studies [18,21] for the characterisation of corrosion pattern is followed. It consists in coupling several analytical techniques (EDS, XRD, μ-Raman) to characterize the corrosion products formed on steel rebars and the nature of steel/concrete interface.

First, optical microscope observations are performed to obtain a global overview of the structure of samples. SEM observations with EDS analyses are conducted to determine chemical composition of the corrosion products. μ-Raman spectroscopy is used to identify the local structure of corrosion products at steel/concrete interface. Moreover, XRD analyses are performed on separate corrosion scales samples taken on rebars to obtain reliable structural information on the different phases of the corrosion products.

3.4.4.1. Samples preparation. A first set of samples is used to characterise the local nature of corrosion products at steel/concrete interface. Samples are taken from concrete cores, mounted in thermo-setting resin and prepared to obtain transversal cross-section with 5-mm thickness. Each sample includes the adhering concrete and the reinforcing steel to characterize the corrosion products in their real exposure environment. Two samples are studied: Sample A taken from "low-corroded" area and Sample B taken from "high-corroded" region in which macroscopic crack is observed. Theses sections are mechanically polished, the final polish is done with 3 and 1 μm diamond grit. Samples preparations (cutting and polishing) are realized using ethanol solution for lubrification. These samples are studied from SEM observations (with EDS X-Ray analyses) and μ-Raman analyses.

A second set of samples is used to obtain structural information on the different phases of the corrosion products (XRD analyses). Corrosion products are sampled on rebars (4 cm in length) with a scalpel and put in powder. As previously,

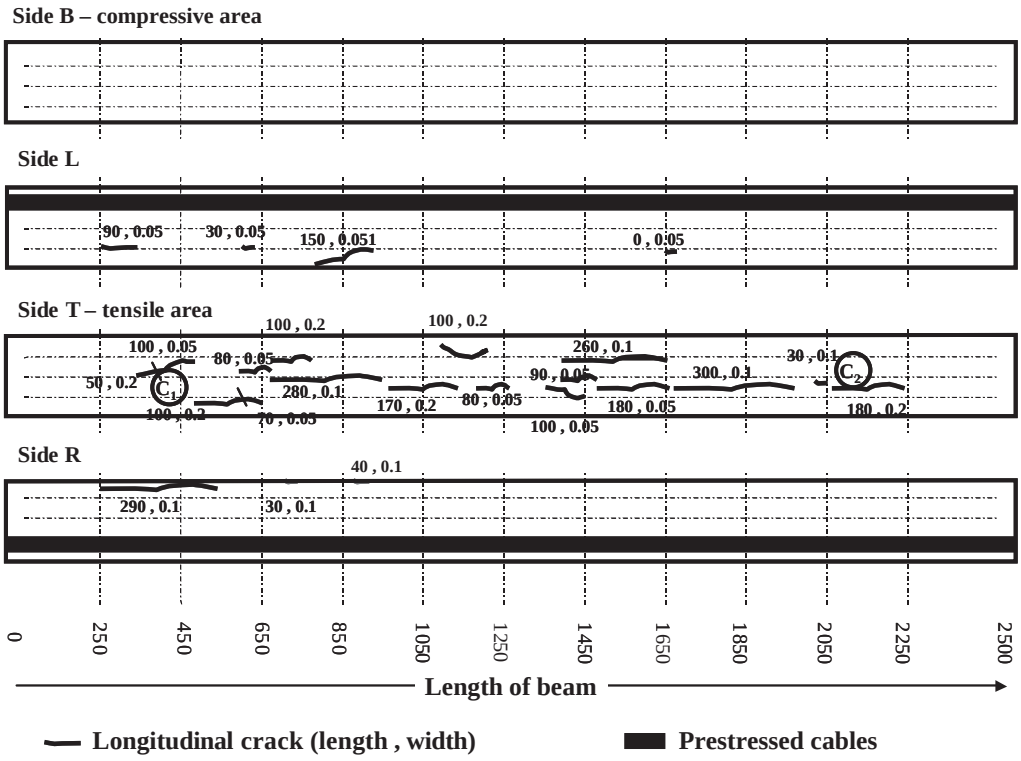

Fig. 3. Crack map — overview of the 4 sides (position of prestressing wires is pointed).

two locations are studied: "low-corroded" area and "high-corroded" area.

3.4.4.2. Characterization techniques. X-ray diffraction (XRD) analyses are performed to obtain information on the crystalline structure of different phases constituting the corrosion products. XRD analyses are obtained on corrosion sample powders with a Siemens D500 diffractometer for 2θ range between 5° and 90°. A cobalt anti-cathode is used (40 kV–30 mA).

Micro-Raman spectroscopy is used to identify the local structure of corrosion products. As a matter of fact, this method notably enables to dissociate magnetite (Fe_3O_4) and maghemite (γ-Fe_2O_3) presenting the same spectrum from XRD analyses [18]. The μ-Raman analyses are performed at LADIR (Laboratoire de Dynamique Interaction et Réactivité – UMR 7075 CNRS–Université Pierre et Marie Curie Paris VI, Thiais, France) on polished cross-section samples used for SEM observations. A Jobin Yvon-Horiba LabRam Infinity spectrometer is used as well as a frequency-doubled Nd:Yag Laser at 532 nm. Measurements are performed with $\times 50$ or $\times 100$ long-focus Leitz objective (with $\times 100$ objective, the beam waist diameter is about 3 μm). As some iron oxides as magnetite are sensitive to laser irradiation

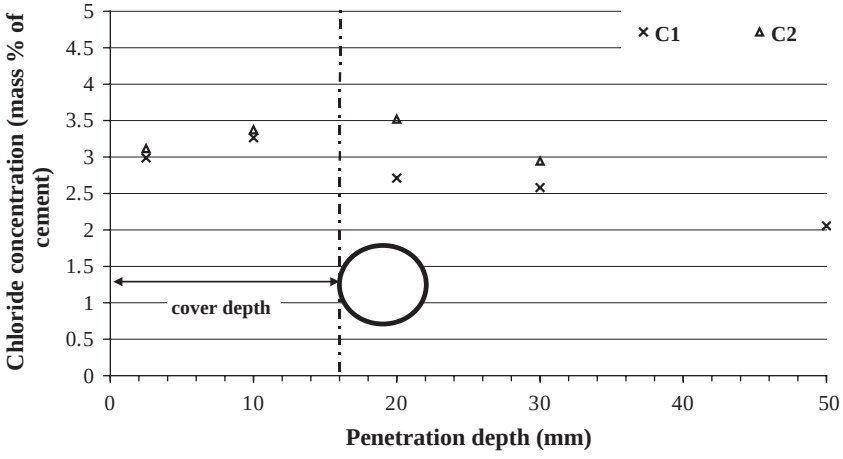

Fig. 4. Acid-soluble chloride concentration (the cover depth for steel is indicated on the graph).

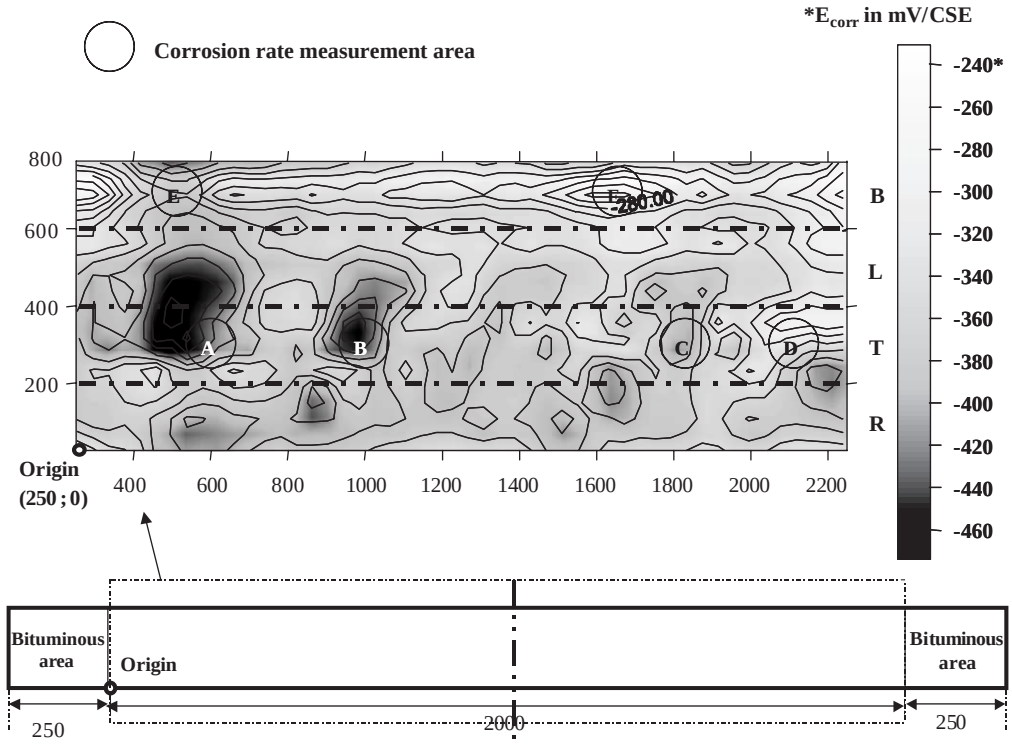

Fig. 5. Half-cell potential map—overview of the 4 sides.

(thermal effect), excitation Laser power on sample is filtered at least below 80 μW (Filters 8 and 80 μW are used in this study).

4. Results and discussion

4.1. Visual observation

A first visual observation enables to propose a global overview of the damage state of the prestressed concrete beam after 40 years exposure in marine environment.

Regarding the concrete characteristic, it is noted the absence of surface damage due to seawater attack and no presence of flexural cracks on the tensile area (upper part) of the beam. Some longitudinal cracks due to corrosion attack can be mainly observed on the side and upper parts (Fig. 3). More precisely it is interesting to note that these longitudinal cracks on Side R and Side L are mainly located on the upper part which correspond to the tensile concrete area. On the contrary, the compressive area (lower side due to the presence of prestressed wires) shows no corrosion induced cracking. Moreover, it can be added that some spots of rust stains appear at some corrosion induced cracks.

4.2. Physico-chemical measurements

Various carbonation measurements are performed on freshly split concrete collected on the different sides along the beam.

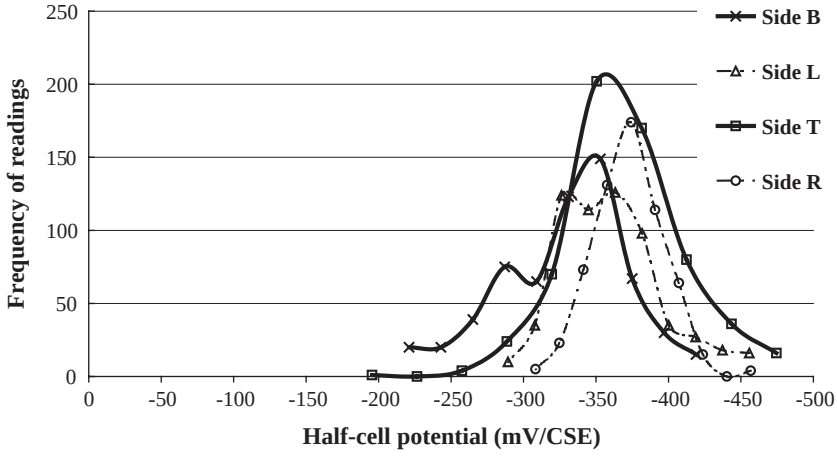

Fig. 6. Frequency distribution of half-cell potential data for the 4 sides of the beam.

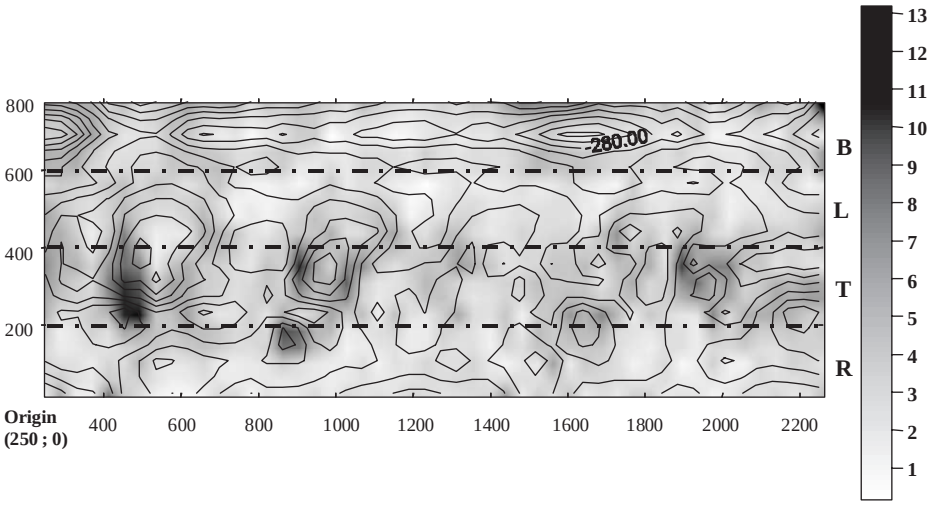

Fig. 7. Potential gradient map—overview of the 4 sides.

For all tests, the maximum carbonation depth is 1 mm. Thus the concrete at the location at 16 mm (cover depth) is not carbonated.

Fig. 4 presents the average profiles of the "total" chloride ion concentration measured at two locations along the beam. A characteristic profile of a concrete structure exposed in tidal marine environment is observed with a maximum value at about 10 mm from the top surface and a slight decrease within bulk structure [22]. At the reinforcing bars depth, the measured values (2.5–3.5% cement mass) exceed the threshold limit (0.5–1.5%) generally pointed out in literature [11,23]. It is generally assumed that for higher chloride content the corrosion by chlorides ions can be initiated at the rebars surface. These results highlight that active corrosion due to chloride ingress can take place at reinforcing steel surface.

4.3. Electrochemical measurements

4.3.1. Half-cell potential

The measurement of the half-cell potential is one of the simplest non destructive methods to indicate the corrosion state of rebars embedded in concrete. However, its interpretation is more delicate. Various approaches are proposed in the literature [14,24].

Fig. 5 illustrates the potential map (the equi-potential contour line plots are indicated) according to a developed view of the beam (dark areas correspond to the most negative potentials). Excepted some spots in the lower part of the beam (side B), half-cell potential readings mainly show absolute values more negative than −0.35 V (/CSE). Considering ASTM C876-9 norm [24] that proposes a correlation between absolute potential values and corrosion activity, this would indicate a high active corrosion probability in the vicinity of all reinforcing bars within structure. However, several studies highlighted that various parameters can modify these absolute potential values without expressing a modification of the corrosion degree at steel surface [14,25]. So an interpretation based on the use of the absolute half-cell potential values may lead to erroneous results on locations of "high-probability" corrosion activity within reinforced concrete structure. That is why we prefer apply the Rilem recommendations which suggest to interpret the half-cell potential values by considering the different potential ranges [14]. The more anodic areas

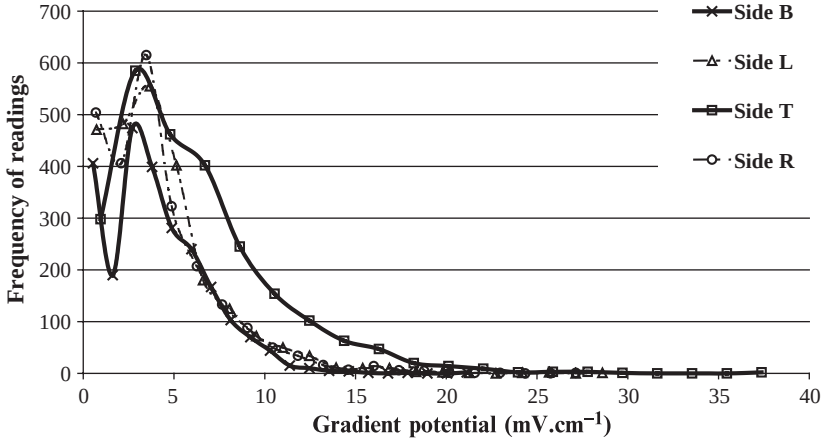

Fig. 8. Frequency distribution of potential gradient data for the 4 sides of the beam.

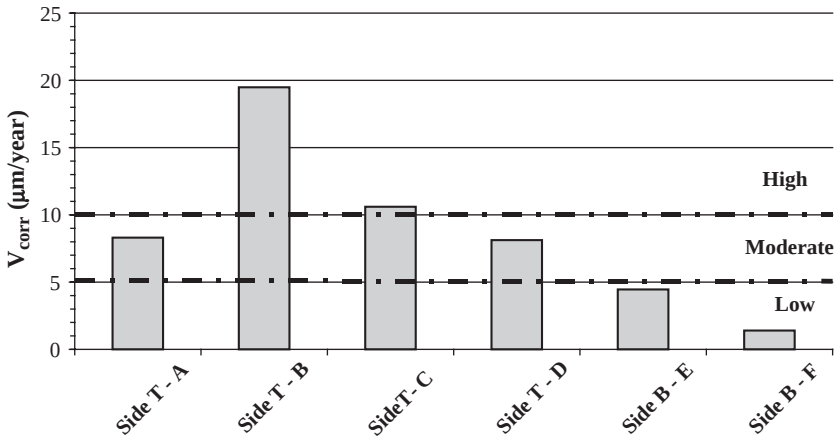

Fig. 9. Corrosion rate values measured on the various locations of the two sides studied.

which could correspond to the areas with the highest corrosion probability are well-identified. Considering potential readings collected on the beam (Fig. 5), only two significant localized anodic areas could be determined respectively at 600 and 1000 mm along the beam on Side L and Side T. Some localized anodic areas can be identified along the beam on Side R.

A complementary way to study half-cell potential readings consists in a statistical analysis. Such analysis allows to compare the corrosion activity of the 4 beam sides. The frequency distributions are illustrated on Fig. 6. Profiles of potential distributions are very close and do not enable to conclude on a different corrosion activity on the four beam sides.

An alternative analysis is proposed based on the estimation of the potential gradient. The spatial variation of half-cell potential gradient is assumed to give some information on the location of higher instantaneous corrosion current [27].

For this purpose, half-cell potential values are used to evaluate the potential gradient (expressed in millivolts per centimeter). Fig. 7 illustrates the potential gradient map (colour plot) (equi-contour line plot represents the potential values). According to this representation, the highest gradient values (corresponding to dark areas) are mainly located in the tensile area of the beam (Side T and in the upper part of the sides L and R). Some localized spots are also noted in the compressive area.

As for half-cell potential values, frequency distributions of potential gradients for each side are illustrated in Fig. 8. Significant differences appear for the four sides. Side T shows clearly higher gradient values compared to the three other sides (bottom, left and right).

4.3.2. Corrosion rate

The analysis of corrosion potential appears to be pertinent to qualify the corrosion activity in reinforced concrete structures. A way to assess the condition of embedded steel reinforcement

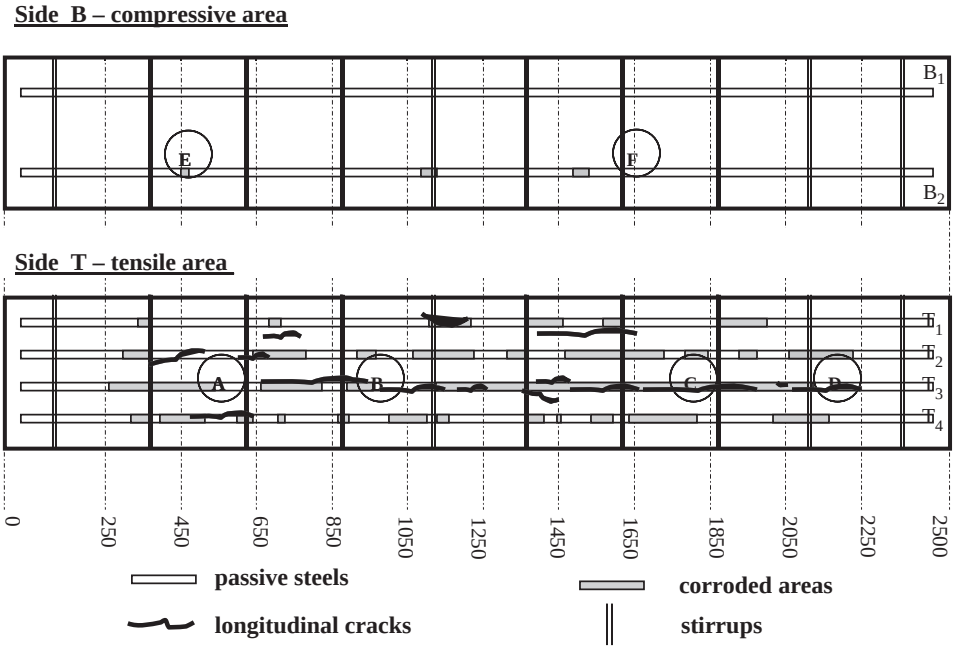

Fig. 10. Distribution of corroded areas on the length of beam for reinforcements in concrete compressive (Side B) and tensile (Side T) areas.

related to its corrosion is also the evaluation of the instantaneous corrosion current density. Measurement areas have been selected on four locations on Side T (Fig. 5). On Side B, as the potential distribution showed a small variation of potential along the beam, only two points are selected (points E and F) (Fig. 5). Fig. 9 illustrates the corrosion values measured on each side (T and B) of the beam. On the same graph, the corrosion level defined according to the Rilem recommendations [15] are indicated.

On one hand, on point measurements located on Side T, corrosion rates vary from 8 to 20 μm/year. These values correspond to moderate to high corrosion level as indicated by the potential gradients. On the other hand, on point measurements located on Side B, corrosion rates vary from 1 to 4 μm/year. These values correspond to low corrosion level.

The results show clearly higher values in the tensile area (upper part, side T) compared to the compressive area (lower part, Side B).

4.4. Distribution of reinforcement cross-section loss

At the end of the non-destructive measurements, concrete cover is removed to examine visually the local corrosion of steel rebars along the beam.

Fig. 10 represents the corrosion spots identified on rebars located in the upper and the lower beam sides. These observations confirm a heterogeneous distribution of corroded areas along the beam (localized corrosion due to chloride ion presence). Moreover measurements of diameter loss are presented in Fig. 11. They confirmed the heterogeneity of the corrosion pattern. A diameter loss of about 30% is noted on the upper part of the beam (equivalent to approximately 50% of steel cross-section). On lower part of the beam (Side B), diameter loss does not exceed 2%. Fig. 12 illustrates the localized corrosion on a length of rebar after removing the corrosion products. These results are in accordance with the corrosion rate evaluation: the corrosion degree is more important in the tensile area of the beam than in its compressive area.

By comparing the longitudinal cracks locations with the corroded areas really observed at steel rebars surface (as indicated in Fig. 10), the correlation between cracks and attack penetration is confirmed as suggested by Rodriguez et al. [26] and Vidal et al. [13] who proposed empirical models to correlate the cracking width and rebar corrosion (cross-section loss). However, this method presents some limits. First, the corrosion areas can be located only when corrosion processes induce enough expansive products to create cracking on the concrete faces. Moreover, existing models to correlate crack width and corrosion are based on empirical relationship in controlled accelerated exposure conditions. More studies have to be performed to generalize models to other exposure conditions (particularly in long term exposure and natural environment).

Electrochemical techniques emerge as accurate non destructive tools to locate and quantify the extension of corrosion damage within reinforced concrete.

Comparing to the visual inspection, it is observed that interpretation of potential map by considering Rilem recommendations enable to locate some anodic areas well-correlated with corroded areas but that other existing corroded area are not well-defined (point D in Fig. 5). An alternative analysis based on the use of gradient potential is proposed. This approach evoked by some authors [27,28] seems to be very pertinent in the way that the local gradient is not influenced by other parameters. For example, the moisture in the rust layer and the electrical continuity at the steel surface can directly influence the intrinsic value of measured potential but not the gradient. As confirmed by visual observation, the higher potential gradient values are mainly located in the upper part of the beam (Side T). The potential gradient seems well-correlated with the real corrosion damage of rebars. Consequently, the use of such a parameter seems more reliable to conclude on the corrosion activity. From results observed from potential gradient map, this approach seems very interesting to locate areas which present higher corrosion activity. This analysis from gradient potential measurement has to be used in the context of additional

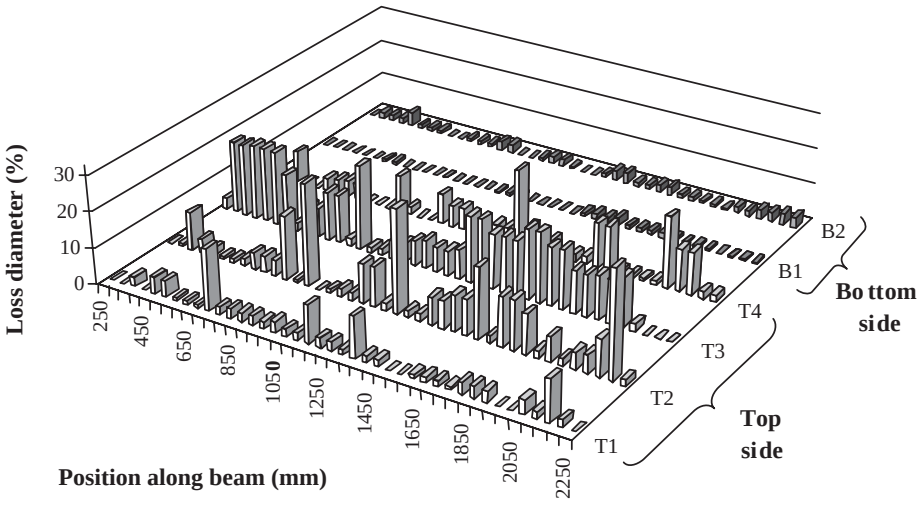

Fig. 11. Diameter loss of passive reinforcements along the beam in tensile area (top side) and in compressive area (bottom side), respectively.

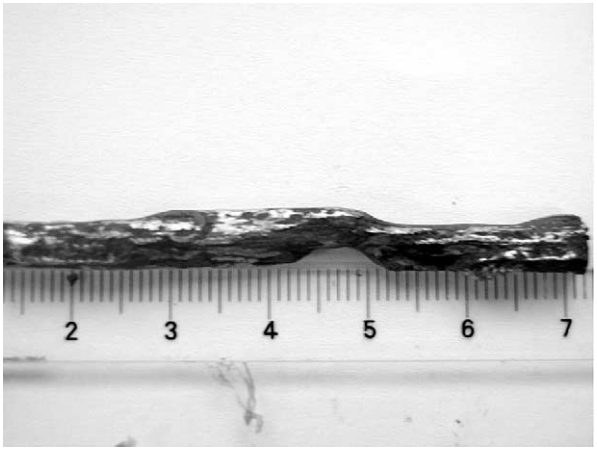

Fig. 12. View of a corroded surface rebar after removing corrosion products.

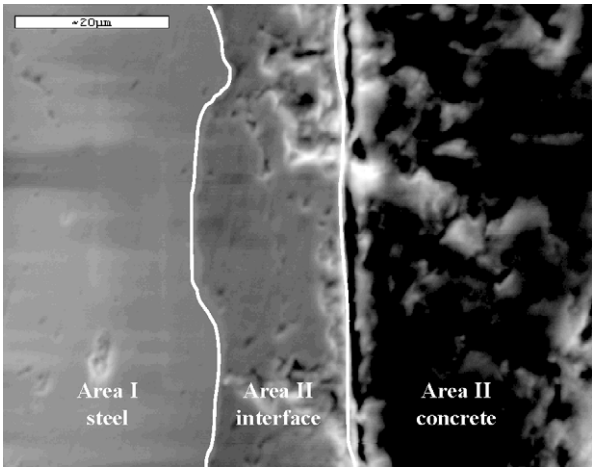

Fig. 14. SEM photography of steel/concrete interface for Sample A (low-corrosion level).

information to conclude on corrosion activity developing within reinforced concrete structure. Use in good conditions and knowing the limits of this method, half-cell potential measurements can be well-adapted to locate the active/passive areas. However, it does not enable to qualify the real damage of rebar: the corrosion rate and consequently the cross section loss cannot be evaluated. This method must be included as a part of the general survey of a corroding structure.

Resistance polarisation measurement is used to evaluate in a quantitative way the corrosion rate and consequently the cross section loss of rebars. Measurements on the two sides of the beam (upper and lower parts) show significantly higher corrosion rate values in the upper part (moderate-high corrosion level according to Rilem recommendation [15]) as confirmed by the results from the other non destructive observations (crack map and potential measurements) and the final observation of rebars after removing the concrete cover. In the lower part of the beam, low corrosion level is estimated. Variations in the values of corrosion rate measured on different locations on a same face can be noticed along the beam. That can be explained by the chloride attack. In chloride contaminated concrete, corrosion is mainly due to pit attack. This corrosion type occurs in localized areas. Prediction and measurement of the polarisation resistance in large concrete structures requires further investigation, especially the application of a guard ring device to limit current spread.

In this study, we have preferred to limit our study on corrosion rate measurement of various locations. No attempt to correlate the evaluated corrosion rate and real mass loss is performed in the way that corrosion rate measurement is instantaneous data which cannot express an average corrosion attack of rebars over a long time exposure. However, as the most damaged zones are close to cracks and crack position is fixed, we can assume that the position of the most corroded zones is fixed. Then the corrosion rate will vary over the seasons with the temperature and humidity, but still we should find a good correlation between the position of the most corroding zones and the maximum corrosion rates.

4.5. Characterisation of corrosion pattern

The autopsy of the beam allows the characterization of the corrosion pattern. Corrosion products taken from two beams areas are investigated: a first one taken from in “low-corroded” area (Sample A) and the second one from a “high-corroded” area (Sample B). Optical microscopic photographies illustrated in Fig. 13 present an overview of the two studied samples cross-sections (steel/concrete system).

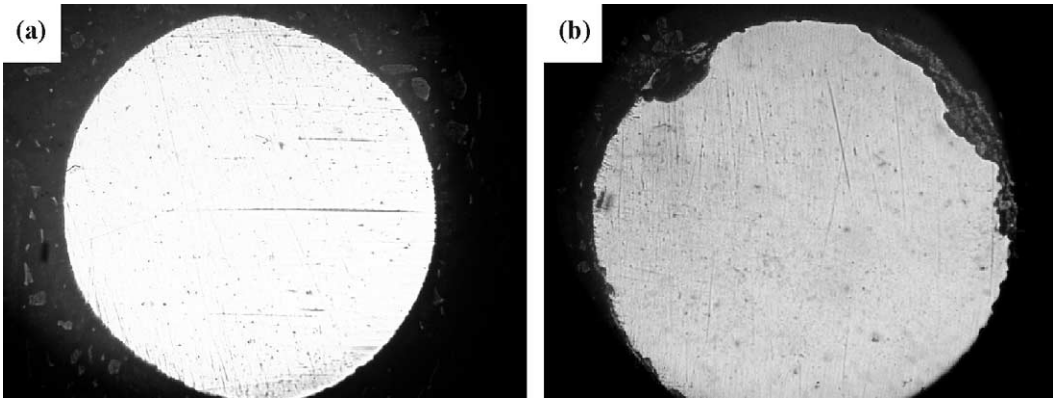

Fig. 13. OM photography of steel/concrete interface (steel diameter is 6 mm). (a) “Low-corroded” sample; (b) “high-corroded” sample.

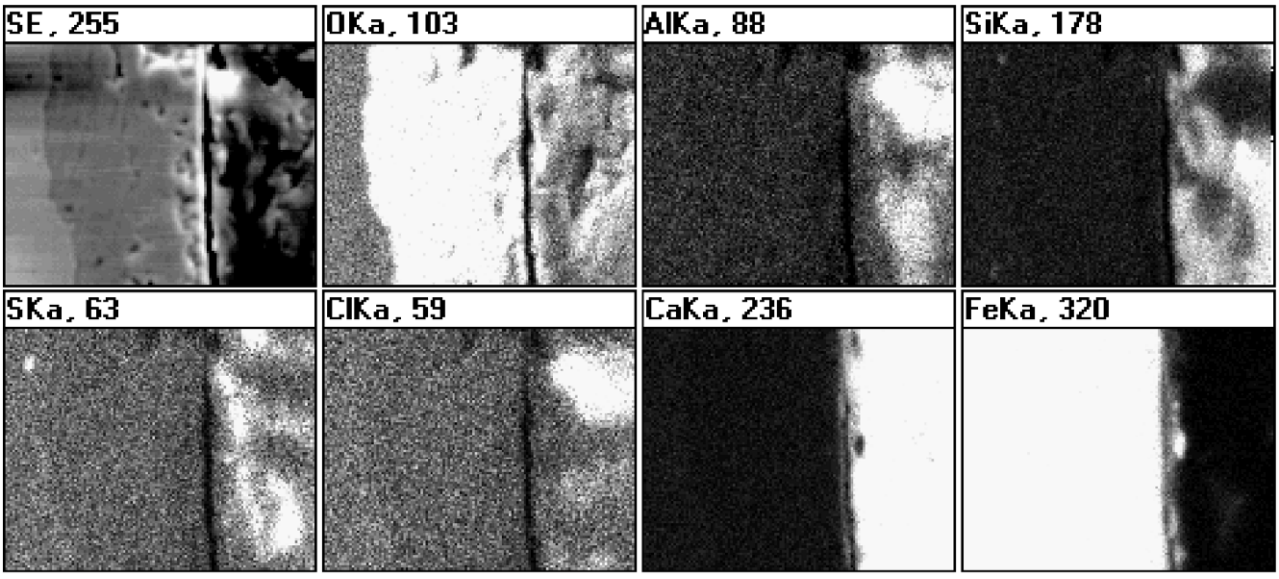

Fig. 15. Elements distribution for steel/concrete interface for Sample A: SE (secondary electron micrograph), O (Oxygen), Al (Aluminium), Si (Silicon), S (Sulfur), Cl (chlorine), Ca (Calcium), and Fe (Iron).

4.5.1. "Low corroded" area—Sample A

4.5.1.1. SEM observations. Cross-section made on Sample A is characterized from SEM observations (Fig. 14). The following corrosion pattern is observed: metallic substrate, corrosion product layer and binder. The corrosion products form a homogeneous layer with 20-μm thickness on all around the reinforcing steel studied on this cross-section.

The X-ray cartography illustrated in Fig. 15 shows the distribution of O, Al, S, Cl, Ca and Fe elements. Steel (Fe) and concrete (Ca, Si, Al, S) are well-identified. It can be noted that some chlorides are identified in concrete at the areas II/III interface. These chlorides are associated with presence of Al elements. During the attack penetration within concrete, some of them were bound with concrete leading to the formation of calcium chloro-aluminate hydrated (Friedel's salt). For this sample, no chlorine phase is observed in the corrosion products layer.

4.5.1.2. XRD analysis. Corrosion products are taken from a 4 cm length rebar with homogenous corrosion layer in surface (no localized area) and put in powder. These rust powder samples are then analyzed by XRD. Results showed dominant peaks of Quartz due to concrete binder and Ferrite due to metallic substrate. Some peaks of goethite (α-FeOOH) and iron oxide (magnetite (Fe_3O_4) or maghemite (γ-Fe_2O_3)) are identified as main corrosion products (Fig. 16). However, these two last oxides cannot be distinguished by XRD because theses diffraction patterns are very close. Moreover, a ferrous hydroxychloride phase (β-$Fe(OH)_3Cl$) is

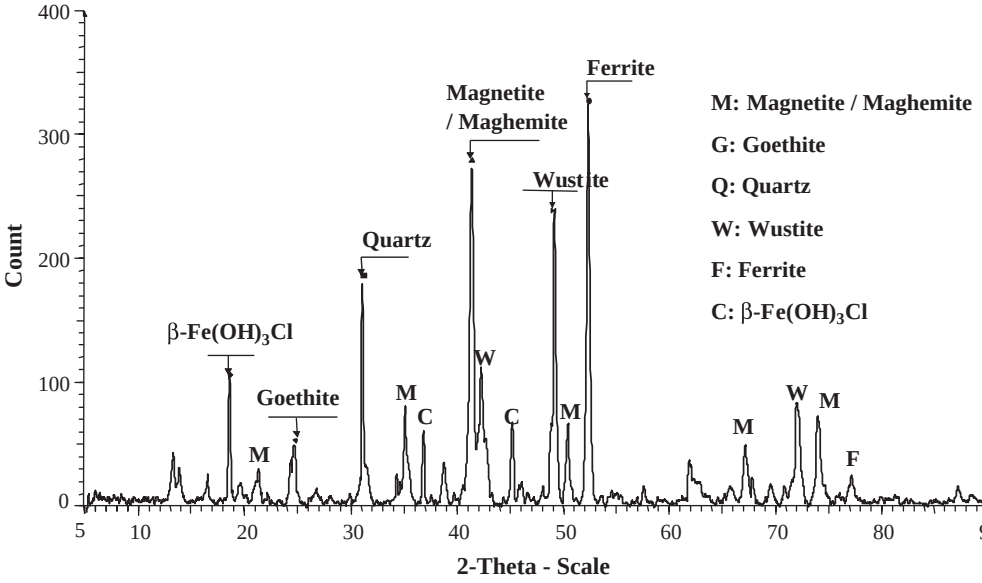

Fig. 16. XRD spectra for "low-corroded" area.

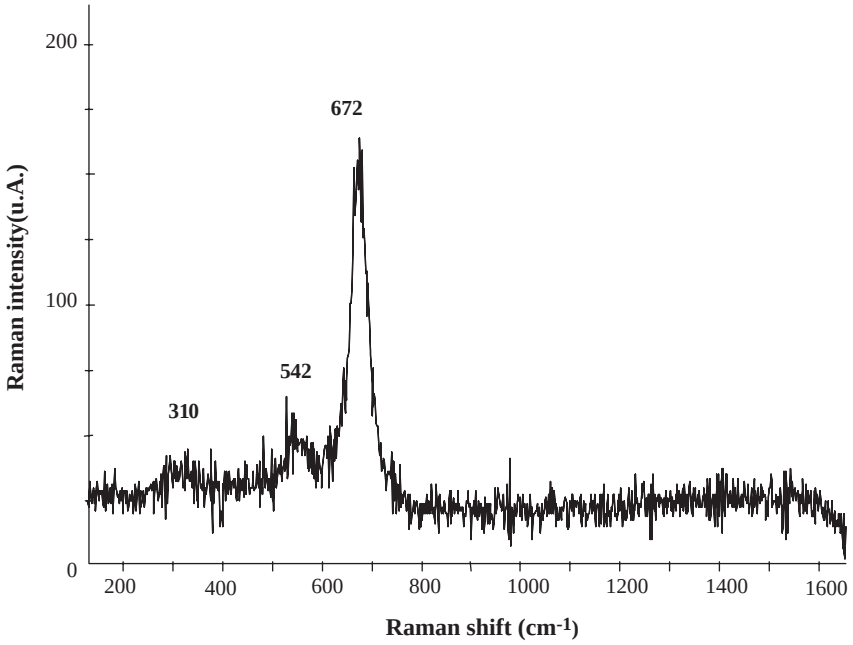

Fig. 17. Phase identified by μ-Raman at steel/concrete interface (Sample A (low-corroded area)) Magnetite–Fe_3O_4.

identified (Fig. 16). This phase has been identified as an intermediate phase to form akaganeite [29]. Secondary elements as wustite (FeO) are identified. Its presence generally observed for high temperature [30] could be explained by experimental procedure adopted to take corrosion products from steel rebars or by its initial presence in metallic substrate as inclusions [18].

4.5.1.3. μ-Raman analysis. Raman micro-spectroscopy is performed to characterize the corrosion products at local scale. In the interface layer observed in Fig. 14, μ-Raman analyses highlight that only magnetite appears (Fig. 17). This phase is identified in the interface area all around reinforcing steel.

It can be suggested that this layer existed when the beams are cast. This pattern can correspond to an initial state of rebars (no relation with corrosion process during long-term exposure) as suggested by Duffo [17].

4.5.2. "High corroded" area — Sample B

4.5.2.1. SEM observations. The optical micrograph of the cross-section made on Sample B show some differences in the steel/concrete interface layer around reinforcing steel bar (Fig. 13(b)). Some pitting occurs around steel rebar. Figs. 18 and 19 illustrate scanning electron micrographs observed on two locations around steel bar (respectively Loc.1 and Loc.2 as precised on Fig. 13(b)). It must be added that a crack in

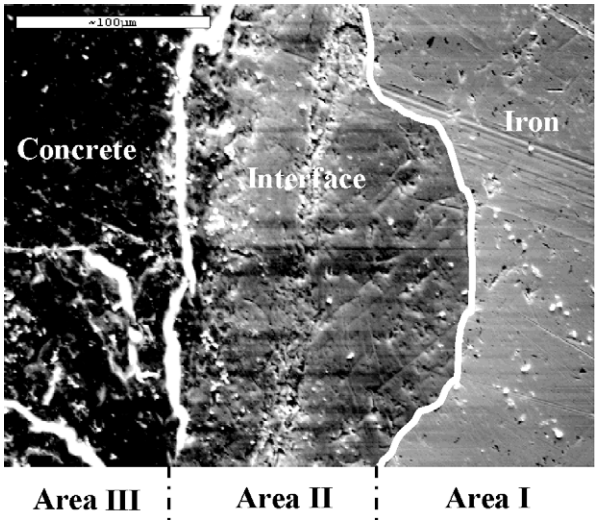

Fig. 18. SEM photography of steel/concrete interface for Sample B — Loc.1 (high-corrosion level).

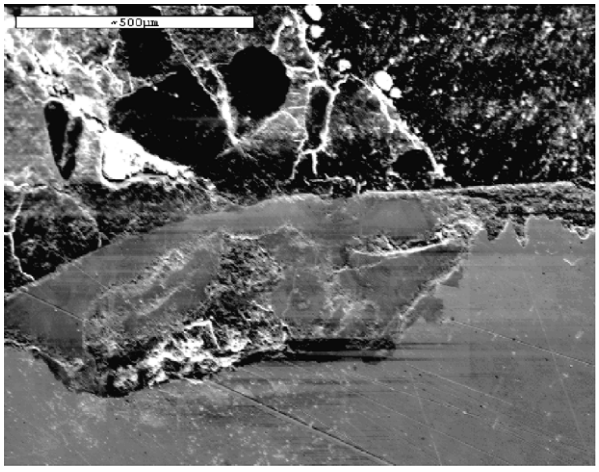

Fig. 19. SEM photography of steel/concrete interface for Sample B — Loc.2 (high-corrosion level).

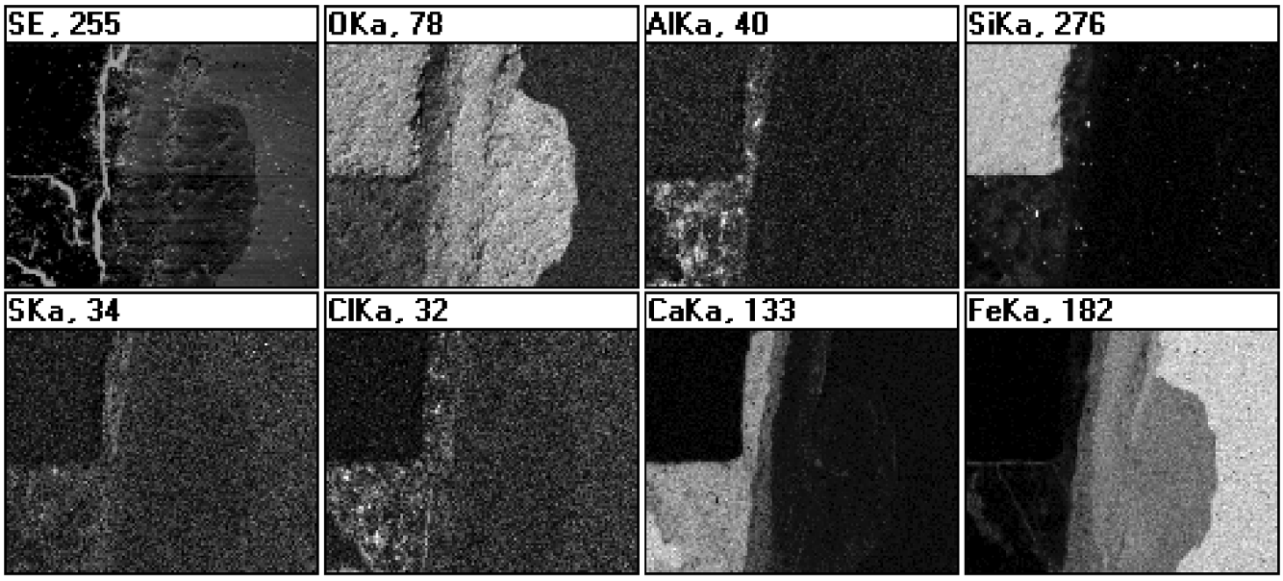

Fig. 20. Elements distribution of steel/concrete interface for Sample B — Loc.1 : SE (secondary electron micrograph), O (Oxygen), Al (Aluminium), Si (Silicon), S (Sulfur), Cl (chlorine), Ca (Calcium), and Fe (Iron).

concrete was observed at the vicinity of the steel/concrete interface near Loc.2.

The general pattern is made of three distinct regions: the metallic iron substrate (Area I), the steel concrete interface (Area II) and concrete (Area III). For the two locations studied on this sample, the thickness of the interface layer is about 100 μm (Fig. 18). Higher values can be observed at some pit locations (Fig. 19).

EDS composition analyses on the two locations allows to identify the elements in each area (Figs. 20 and 21). Area I is mainly composed of Fe (metallic substrate). In Area III, aggregates are well identified by Ca and Si. The presence of Si and O indicates quartz grains. Finally the rust layer (Area II) is mainly constituted of iron and oxygen. It can be noted from analysis performed on Loc.1 (Fig. 20) that some chlorides are identified in concrete at the areas II/III interface. These chlorides are associated with presence of Al elements, as previously observed in zone "A" (low corroded area).

However, EDS analyses performed on Loc.2 clearly indicate the presence of chloride elements within corrosion product layer at the vicinity of steel substrate (at the end of the pit) (Fig. 21).

4.5.2.2. XRD analysis. Corrosion products are taken from a 4 cm length rebar with a localized corrosion layer in surface (Sample B, high-corrosion level) and put in powder. As previously observed, results show dominant peaks of

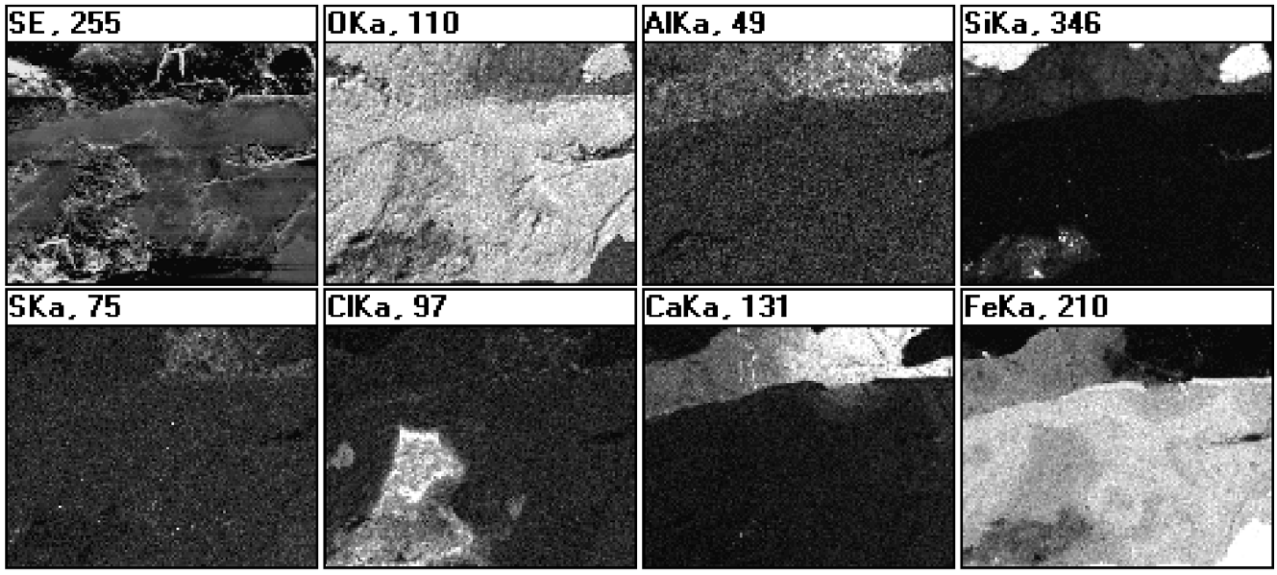

Fig. 21. Elements distribution of steel/concrete interface for Sample B — Loc.2: SE (secondary electron micrograph), O (Oxygen), Al (Aluminium), Si (Silicon), S (Sulfur), Cl (chloride), Ca (Calcium), and Fe (Iron).

goethite (α-FeOOH) and iron oxide (magnetite (Fe_3O_4) or maghemite (γ-Fe_2O_3)) (Fig. 22). Peaks of Quartz due to presence of concrete is observed. Moreover, a significant "akaganeite" peak (β-FOOH) is noticed. This phase is characteristic of chloride ions presence in the corrosion process [30]. Some secondary elements as bernalite ($Fe(OH)_3$) are also observed.

The presence of goethite and magnetite as corrosion products after long-term exposure within reinforced concrete structures have been confirmed in previous studies [17,18].

4.5.2.3. μ-Raman analysis. The local structure of the corrosion product layer is characterized by μ-Raman. Its morphology can be decomposed into two distinct layers. In contact with the steel (Area II-a), a homogeneous layer of goethite is observed. The outer layer (Area II-b) present a heterogeneous mix with mainly iron-oxide phase in which very localized presence of goethite is observed (Fig. 23(b)). It is interesting to note that μ-Raman analysis precised that the iron oxide formed in the outer layer is Maghemite (γ-Fe_2O_3) (Fig. 23(a)). Therefore, it is more likely that the peaks (reflection lines) observed in the X-ray diffraction spectra (Fig. 22(b)) are due to maghemite rather than to magnetite.

The presence of maghemite can be explained by oxidation of magnetite due to the diffusion of oxygen through the pores within concrete and in the oxide layer during the wetting/drying cycle.

μ-Raman analyses confirm the presence of the β-iron oxy-hydroxide, akaganeite, on some locations around the rebar at the oxide/steel interface due to chloride attack (Fig. 24).

On the two samples studied, some differences are found between "low-corroded" and "high-corroded" level areas on their corrosion pattern.

When the corrosion process is activated on some locations of the steel surface due to chloride ions presence, the interface layer is largely modified (Sample B). Fig. 25 describes a schematic view of corrosion pattern. A layer made of goethite is in contact with the steel (inner layer). A second layer (outer layer) in contact with concrete appears composed of maghemite with some spots of goethite.

As observed by Chitty et al. [18] on archaeological artefacts, it is interesting to note that, in the "high-corroded" area, the only corrosion products observed close to metallic substrate are oxy-hydroxides with valence III+(goethite).

Concerning the corrosion pattern, some differences with the previous studies are noted in the characterisation of the corrosion products at a microscopic scale. No transformed medium as observed by Chitty et al. [18] is detected at the corrosion product layer/concrete interface.

5. Conclusion

This paper presents diagnosis results of the corrosion damage of a prestressed concrete beam after 40 years exposure in marine environment is suggested.

Physico-chemical measurements have confirmed that chloride ions are the only responsible of corrosion attack. The comparison of the results issue from non destructive methods with visual observation of reinforcing steels has allowed to establish the following conclusions:

- crack map gives a global overview of the corrosion area (but only when the corrosion process reaches a critical issue),
- potential gradient measurement method is very attractive to locate the corroding area within concrete structure,

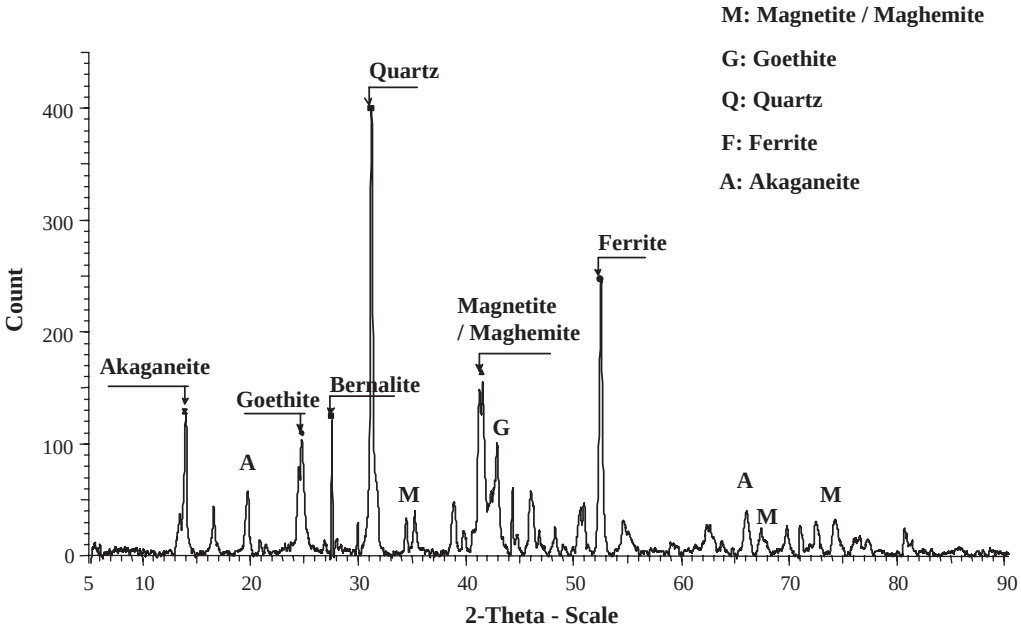

Fig. 22. XRD spectra for "high-corroded" area (Sample B).

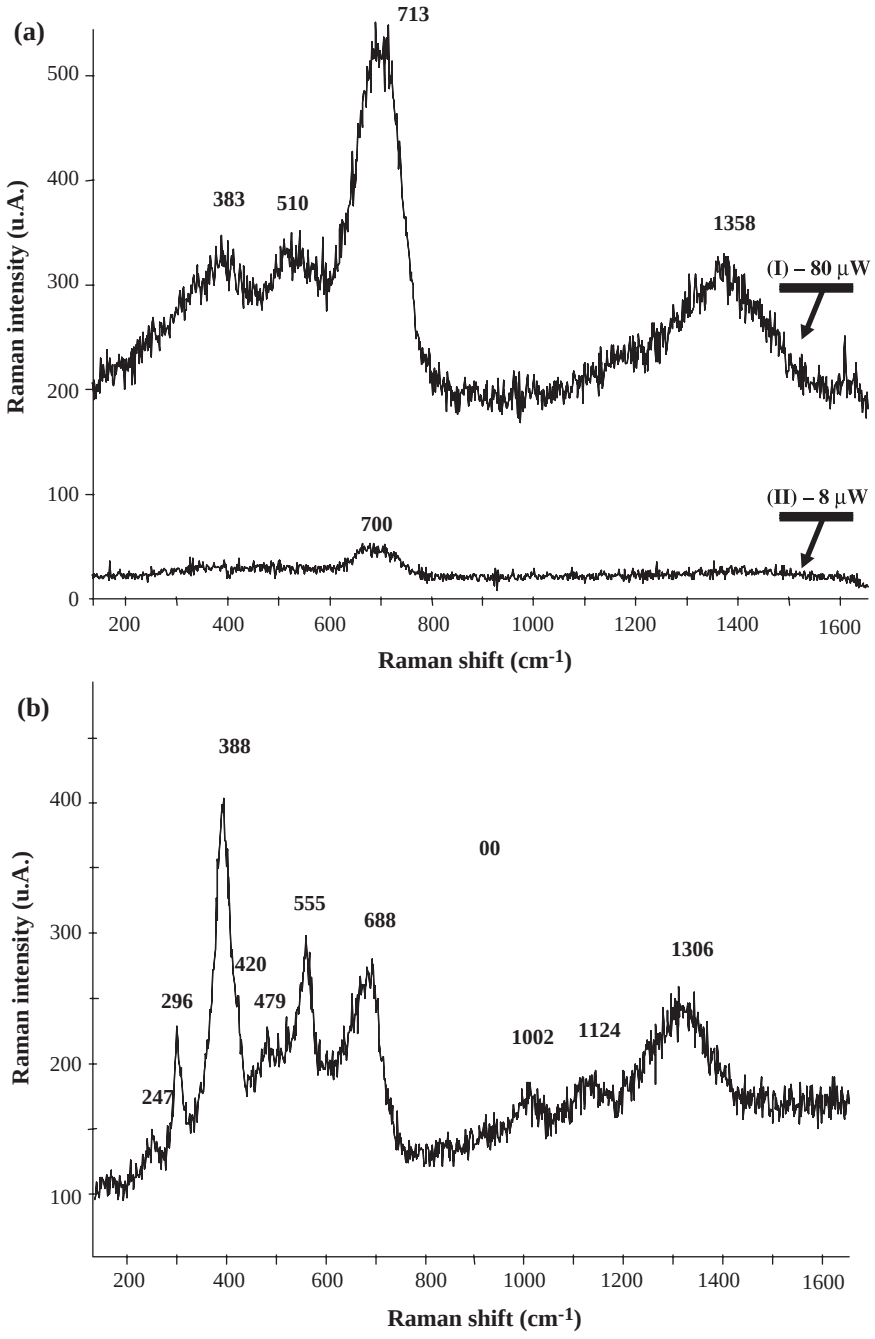

Fig. 23. Main phase identified by μ-Raman at steel/concrete interface. (a) Maghemite γ-Fe_2O_3—(I) Filter 80 μW, (II) Filter 8 μW. (b) Goethite—α-FeOOH.

– corrosion rate measurements confirmed the corrosion damage risks within concrete beam.

However, non destructive measurements as confirmed by visual observation suggest an heterogeneous corrosion along the rebar surface. That can be explained by the electrochemical nature of chloride corrosion process which tends to be localized forming active zones of dissolving metal and passive areas (macro-cell effect) [31,32]. Moreover, it is evident that corrosion activities within the beam are different depending on the locations within the beam. Considering the results of the different non destructive methods tested during this research project, conclusion on an "active" corrosion in the upper part of the beam and a "low" corrosion in the lower part can be made with confidence. These observations are confirmed by visual inspection after removing the concrete. Diameter loss measurements have shown a significant difference of corrosion activity within the beam between the lower part (lower activity) and the upper part (higher activity) of the beam. That can be explained by various factors. First, tensile/compressive stresses within the concrete structure have a significant effect on corrosion of passive reinforcing steel. As proposed by Francois and Arliguie [12], this difference can be attributed to micro-cracking which may occur in tensile zones of reinforced

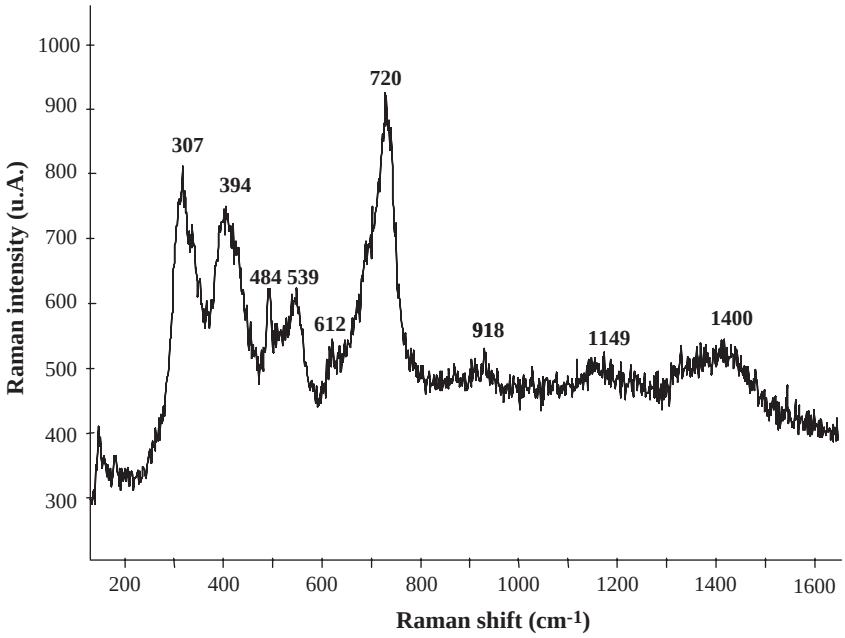

Fig. 24. Chloride associated phase identified by μ-Raman at steel/concrete interface. Akaganeite β-FOOH.

concrete beam (in our study case, the upper part due to position of prestressing wires within the beam). That can imply an increase in chloride and oxygen penetration within the concrete and damage at steel/concrete interface. A second point must be highlighted. The tensile side of the beam is also the upper side according to casting direction. Then, the possible effect of bleeding and settling of fresh concrete on the interface quality (formation of void) can also explain a part of the difference of corrosion activity between upper and lower sides as already highlighted in the literature [33].

Finally steel/concrete interface has been studied from macro- and micro-levels characterization methods to improve the understanding of the corrosion system which forms after long-time exposure. The following corrosion pattern is observed: metallic substrate, corrosion product layer and concrete. The coupling of these techniques has allowed the identification and localisation of corrosion products. Composition and thickness of the corrosion product layer varies with the damage degree. For "low-corroded" regions (some micrometers in thickness), corrosion product layer is only composed of magnetite. For "high-corroded" regions, corrosion product layer (some 500 μm in thickness) is mainly composed of goethite and maghemite. Akaganeite is present at the corrosion product/metallic substrate interface in some pits.

Given the fact that the "high-corroded zones" were detected close to cracks and that their morphology is different with respect of the "low corroded zones," one may conclude, that their position did not shift in time.

These results will be used for modelling the chloride-induced corrosion mechanisms in the reinforced concrete after a long-term exposure in natural environment.

Acknowledgements

The authors acknowledge the French Ministry of National Education, Research and Technology for its financial support. The study is part of a RGCU (Urban and Civil Engineering Network) program, "Benchmark des poutres de La Rance" and CIMETAL program (French Atomic Energy Commission (CEA), Electricité De France EDF)).

The authors are grateful to N. Da Silva and A. Patureau (CEBTP) for potential measurements, to W. Guillot (CEA) and

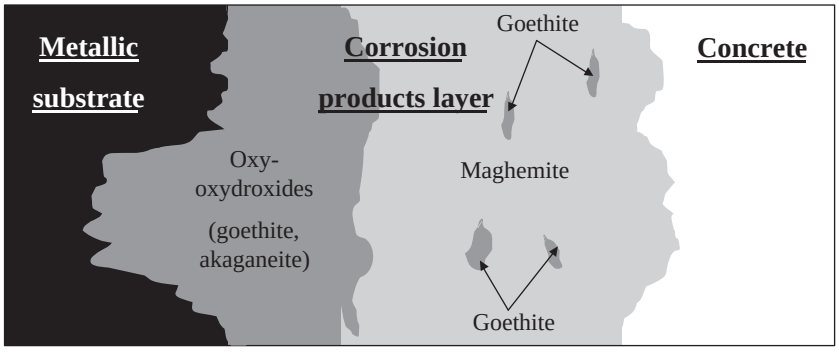

Fig. 25. Schematic description of the corrosion layer structure for Sample B.

L. Bellot-Gurlet (LADIR) for their help for XRD and μ-Raman experiments.

References

[1] K. Tuutti, Corrosion of Steel in Concrete, CBI Research Report no. 4.82, Swedish Cement and Concrete Research Institute, Stockholm, Sweden, 1982.
[2] A. Neville, ACI Mater. Struct. 28 (1995) 63.
[3] M.F. Montemor, A.M.P. Simoes, M.G.S. Ferreira, Cem. Concr. Compos. 25 (2003) 491.
[4] S. Ahmad, Cem. Concr. Compos. 25 (2003) 459.
[5] A. Castel, R. François, G. Arliguie, Mater. Struct. 33 (2000) 539.
[6] J. Rodriguez, L.M. Ortega, J. Casal, Constr. Build. Mater. 11 (4) (1997) 239.
[7] J. Avila-Mendoza, J.M. Flores, U.C. Castillo, Corrosion 50 (11) (1994) 879.
[8] KK. Sagoe-Crentsil, F.P. Glasser, Corrosion 49 (6) (1994) 457.
[9] C. Andrade, M. Keddam, X.R. Novoa, M.C. Perez, C.M. Rangel, H. Takenouti, Electrochim. Acta 46 (2001) 3905.
[10] M. Moreno, W. Morris, M.G. Alvarez, G.S. Duffo, Corros. Sci. 46 (11) (2004) 2681.
[11] C. Alonso, C. Andrade, M. Castellote, P. Castro, Cem. Concr. Res. 30 (7) (2000) 1047.
[12] R. François, G. Arliguie, Mag. Concr. Res. 51 (2) (1999) 143.
[13] T. Vidal, A. Castel, R. François, Cem. Concr. Res. 34 (1) (2004) 165.
[14] RILEM TC 154-EMC, Mater. Struct. 36 (2003) 461.
[15] RILEM TC 154-EMC, Mater. Struct. 37 (2004) 623.
[16] D.W. Law, J. Cairns, S.G. Millard, J.H. Bungey, NDT E Int. 37 (2004) 381.
[17] G.S. Duffo, W. Morris, I. Raspini, C. Saragovi, Corros. Sci. 46 (2004) 2143.
[18] W.J. Chitty, P. Dillmann, V. L'Hostis, C. Lombard, Corros. Sci. 47 (6) (2005) 1555.
[19] M. Castellote, C. Andrade, Mater. Struct. 34 (2001) 532.
[20] M. Stern, A.L. Geary, J. Electrochem. Soc. 104 (1957) 56.
[21] D. Neff, S. Reguer, L. Bellot-Gurlet, Ph. Dillmann, R. Bertholon, J. Raman Spectrosc. 35 (8–9) (2004) 739.
[22] A. Lindvall, Environmental actions on concrete exposed in marine and road environments and its response: consequences for the initiation of chloride induced reinforcement corrosion, PhD dissertation, 2003, Chalmers Univ. of Techn., 233 pages, Sweden.
[23] RILEM TC 124-SRC, Mater. Struct. 27 (1994) 415.
[24] Standard Test Method for Half-Cell Potentials of Uncoated Reinforcing Steel in Concrete, ASTM C 876-91 (1991).
[25] G. Grimaldi, P. Brevet, G. Pannier, A. Raharinaivo, Br. Corros. J. 21 (1) (1986) 55.
[26] J. Rodriguez, L.M. Ortega, J. Casal, J.M. Diez, Conference on Durability of Buildings Materials and Components, vol. 1, 1996, p. 117.
[27] I. Medgyesi, J. Berecz, A. Jantai, M. Kelemen, Bull. Liaison LCPC 158 (1988) 29.
[28] C.M. Hansson, Cem. Concr. Res. 14 (1984) 574.
[29] S. Reguer, P. Dillmann, F. Mirambet, L. Bello-Gurlet, in press.
[30] R.M. Cornell, U. Schwertmann, The Iron Oxides: Structures, Properties, Reactions, Occurrences and Uses, Ed. Wiley, second, completely revised and extended edition, 2003.
[31] S.C. Kranc, A. Sagues, Corros. Sci. (2001) 1355.
[32] B. Elsener, Cem. Concr. Compos. 24 (2002) 65.
[33] T.A. Soylev, R. François, Cem. Concr. Res. 33 (9) (2003) 1407.